Plasma Sources Sci. Technol. **9** (2000) 45–56. Printed in the UK PII: S0963-0252(00)09005-8

Transitions and scaling laws for electronegative discharge models

A J Lichtenberg†, M A Lieberman†, I G Kouznetsov† and T H Chung‡

† Department of Electrical Engineering and Computer Sciences, University of California, Berkeley, CA 94720, USA
‡ Department of Physics, Dong-A University, Pusan 604-714, Korea

Received 3 December 1998, in final form 1 September 1999

Abstract. The equilibrium of electronegative discharges is studied in the plane-parallel approximation over a wide range of pressures and electron densities, encompassing a number of regimes that have previously been modeled analytically. The transitions between the various regimes (models) have been determined in the input parameter space. It is shown that for a given feedstock gas, these transitions can be found in terms of the two input parameters $p\ell_p$ and $n_{e0}\ell_p$, where p is the pressure, n_{e0} the electron density, and ℓ_p the system half-length. Here n_{e0} is used as a convenient input related to the power, and the conversion from electron power to n_{e0} is given. The input parameter space is partitioned by whether ion flux to the wall or positive–negative ion recombination is the dominant positive ion loss mechanism. For each of the principal regimes, scaling laws are developed for the most important plasma parameters in terms of the input parameters.

1. Introduction

Plasma processing involves electronegative gas mixtures. The number of equations governing the equilibrium is large and analysis becomes complicated. At the same time there is an increased need to understand the scaling of the plasma constituents with control parameters, since the parameter space is much enlarged from that of electropositive plasmas. In an early study of an electronegative positive column the continuity and force equations for a three-species plasma, consisting of electrons, one positive ion, and one negative ion species, were solved numerically to obtain the equilibrium [1]. These numerical results give little insight into the importance of various terms in the equations and the scaling with parameters. More recent numerical work using fluid codes [2–4] and particle-in-cell simulations [5, 6] have determined plasma properties at single points within the parameter space or scaling over limited ranges of parameters. However, these codes are computer intensive and it is therefore very time and resource consuming to explore all interesting parameter ranges.

An alternative approach to determine the plasma equilibrium is to employ simplifying assumptions. The equilibrium parameters can then be connected to the equations describing the heating mechanism to give a complete description. In the simplest of equilibrium models all quantities are taken to be averages over the spatial variables, and are therefore called point models or *global* models. Such models are easy to use and can incorporate additional positive and negative ion species [7–9]. The assumptions that are used in the averaging process are generally not uniform over the phase space, making it difficulty to determine the model accuracy, or to distinguish the scaling across various parameter regimes.

Another model for the equilibrium retains the spatial variations, but employs sufficient simplifying assumptions that solutions can be obtained [10–17]. As with the global models, it is essential to determine the range of validity of the approximations that are made. This procedure for simplifying the analysis, which also uncovers the basic structure of the discharge, was developed by Tsendin [11] to treat a cylindrical dc discharge. In that work it was recognized that the discharge would naturally stratify into two regions: an electronegative core in which essentially all of the negative ions would concentrate, and an electropositive edge. The physical mechanism of this stratification was investigated in [12]. However, the resulting equations were still quite complicated such that further simplifications were required for analysis. In particular, detachment rather than recombination was considered to be the main process for removing negative ions, thus linearizing the coupled equations. The usually more important process of recombination was considered briefly in [11], and in more detail in [14], resulting in nonlinear equations that did not make the scalings transparent. In an alternative simplification, Lichtenberg *et al* [15] further reduced the problem by using the approximation that the negative ions, as well as the electrons, are in Boltzmann equilibrium. In this situation the electron profile is nearly constant, and a single ambipolar diffusion equation can be constructed to describe the equilibrium. Approximation solutions, originally constructed at intermediate pressures at which the core electronegative region and the edge electropositive region have nearly constant (but different) ambipolar diffusion

coefficients, were extended to lower pressure for which the electropositive diffusion coefficient varied with position [16]. In this work the effect of the positive ion diffusion velocity reaching the local ion sound velocity within the electronegative core was also considered.

In another paper [17] the previous work on three-species, spatially non-uniform plasma was extended to higher electronegativity, in which the positive–negative ion recombination may dominate the diffusive flow loss and for which the basic assumption of Boltzmann negative ions may not hold. At higher pressure the electronegative core has an elliptic rather than a parabolic profile, which can be approximated by a profile with a flat region at its centre. At high electronegativity the electropositive edge can also disappear. The basic equations in [17], without the Boltzmann assumption for negative ions, were also solved numerically in [14], in cylindrical geometry, near the transition between elliptic and parabolic profiles.

The purpose of this study is to review the models that have been developed for the various parameter regions [15–17], to determine the transitions between the regimes, and to obtain scaling laws for each of the principal regimes. For justification of the approximations the reader is referred to the previous papers [15–17]. For equilibrium models, with a given feedstock gas, the control parameter space consists of two parameters $p\ell_p$ and $n_{e0}\ell_p$ where p is the pressure, n_{e0} is the central electron density and ℓ_p is the half length of the plasma. The discharge parameters to be examined are the ratio of the centre negative ion density to electron density $\alpha_0 = n_{-0}/n_{e0}$, the fractional half-length of the electronegative region ℓ/ℓ_p, and a scale length of an assumed profile to be determined for various models. The ratio of the recombination flux to the positive ion diffusion flux leaving the discharge, $\Gamma_{rec}/\Gamma_+(\ell_p)$, is an important subsidiary parameter, used to separate equilibrium regimes. For particular types of discharges the input power or some other electrical quantity may be chosen as a control parameter. In this situation it may also be necessary to consider heating mechanisms and sheath models [18], which we do not consider in this study of equilibria.

2. Basic formalism

As in electropositive plasmas, for each charged species we can write a flux equation

$$\begin{aligned}\Gamma_+ &= -D_+\nabla n_+ + n_+\mu_+E\\ \Gamma_- &= -D_-\nabla n_- - n_-\mu_-E\\ \Gamma_e &= -D_e\nabla n_e - n_e\mu_eE\end{aligned} \tag{2.1}$$

where the symbols have their usual meanings, and the subscripts +, −, and e denote positive ions, negative ions, and electrons, respectively. In equilibrium the sum of the currents must balance:

$$\Gamma_+ = \Gamma_- + \Gamma_e. \tag{2.2}$$

We also have

$$n_+ = n_- + n_e \tag{2.3}$$

which is the usual quasineutral plasma approximation. In this approximation we consider the pressure to be sufficiently high that a constant mobility model is appropriate, which is generally adequate when negative ions are present, but the pressure is not so high that the electron mean free path is short compared to the system size such that non-uniform heating leads to a non-uniform temperature. We form a set of coupled differential equations using the continuity equations for each species

$$\nabla\cdot\Gamma_i = G_i - L_i \tag{2.4}$$

where G_i are the sources and L_i are the sinks. Since the electrons are very mobile, in the bulk plasma we can eliminate the electric field by use of a Boltzmann assumption for the electrons

$$D_e\nabla n_e + \mu_e n_e E \simeq 0 \tag{2.5}$$

i.e. that both terms in (2.5) are large compared to the flux; this holds for a ratio of negative ion density to electron density, satisfying $\alpha \equiv n_-/n_e < \mu_e/\mu_-$ [17].

At relatively high electronegativity α, if (2.5) holds but if the negative ions are not in Boltzmann equilibrium with the potential (see (2.26)), we combine the flux and continuity equations to obtain a pair of differential equations which in plane-parallel geometry are

$$\frac{\mathrm{d}}{\mathrm{d}x}\left(-D_+\frac{\mathrm{d}n_+}{\mathrm{d}x} + n_+\mu_+E\right) = K_{iz}n_gn_e - K_{rec}n_+n_- \tag{2.6}$$

and

$$\frac{\mathrm{d}}{\mathrm{d}x}\left(-D_-\frac{\mathrm{d}n_+}{\mathrm{d}x} - n_-\mu_-E\right) = K_{att}n_gn_e - K_{rec}n_+n_-. \tag{2.7}$$

Here n_g is the neutral gas density, K_{iz} is the ionization rate constant, K_{rec} is the recombination rate constant, K_{att} is the dissociative attachment rate constant, and we have only retained the dominant reactions. The electric field and the density of one species may be eliminated using the Boltzmann relation (2.5) for electrons and the plasma approximation (2.4) of charge neutrality. Making these substitutions, and taking $\mu_- = \mu_+$ and $D_- = D_+$ ($T_- = T_+ \equiv T_i$) for simplicity, we obtain

$$\begin{aligned}&\frac{\mathrm{d}}{\mathrm{d}x}\left(-D_+\frac{\mathrm{d}}{\mathrm{d}x}(n_- + n_e) - \mu_+(n_- + n_e)T_e\frac{1}{n_e}\frac{\mathrm{d}n_e}{\mathrm{d}x}\right)\\ &\quad = K_{iz}n_gn_e - K_{rec}(n_- + n_e)n_-\end{aligned} \tag{2.8}$$

and

$$\begin{aligned}&\frac{\mathrm{d}}{\mathrm{d}x}\left(-D_+\frac{\mathrm{d}n_-}{\mathrm{d}x} + \mu_+n_-T_e\frac{1}{n_e}\frac{\mathrm{d}n_e}{\mathrm{d}x}\right)\\ &\quad = K_{att}n_gn_e - K_{rec}(n_- + n_e)n_-\end{aligned} \tag{2.9}$$

where we have used the Einstein relations [18] to write $D_e/\mu_e = T_e$. Equations (2.8) and (2.9) can be solved simultaneously, together with the appropriate boundary conditions, to obtain the density profiles.

2.1. Boltzmann equilibrium for negative ions

If we make the more restrictive assumption that the negative ion species is also in Boltzmann equilibrium, then [18]

$$\frac{\nabla n_-}{n_-} = \gamma\frac{\nabla n_e}{n_e} \tag{2.10}$$

where $\gamma = T_e/T_i$ (T_i is the common temperature of the ionic species). Using (2.10) together with

$$\nabla n_+ = \nabla n_- + \nabla n_e$$

we obtain the ratios

$$\frac{\nabla n_e}{\nabla n_+} = \frac{1}{1+\gamma\alpha} \qquad \frac{\nabla n_-}{\nabla n_+} = \frac{\gamma\alpha}{1+\gamma\alpha}. \tag{2.11}$$

Substituting (2.2) and (2.11), together with the Einstein relations [18]

$$\frac{D_-}{D_+} = \frac{\mu_-}{\mu_+} \qquad \frac{D_e}{D_+} = \gamma\frac{\mu_e}{\mu_+}$$

into (2.1), we can eliminate n_- and n_e to obtain, after some algebra, an equation for the positive ion flux in terms of n_+ alone,

$$\Gamma_+ = -D_{a+}\nabla n_+ \tag{2.12}$$

where we now have, analogous to electropositive plasmas, an ambipolar diffusion coefficient

$$D_{a+} = D_+\frac{(1+\gamma+2\gamma\alpha)(1+\alpha(\mu_-/\mu_e))}{(1+\gamma\alpha)(1+(\mu_+/\mu_e)(1+\alpha)+\alpha(\mu_-/\mu_e))} \tag{2.13}$$

which is the form given by Thompson [19]. We note immediately, since μ_-/μ_e, $\mu_+/\mu_e \ll 1$, that except at very high α the second parentheses in both the numerator and denominator are approximately equal to one, yielding

$$D_{a+} \approx D_+\frac{1+\gamma+2\gamma\alpha}{1+\gamma\alpha}. \tag{2.14}$$

This simpler form of D_{a+} can be obtained directly, by substituting (2.11) into (2.8). Thompson plotted D_{a+} from (2.13) with α as a parameter. The structure is easily seen from the simpler form (2.14). For $\alpha \gg 1$, γ cancels such that $D_{a+} \approx 2D_+$. When α decreases below unity, but $\gamma\alpha \gg 1$ then $D_{a+} \approx D_+/\alpha$ such that D_{a+} increases with decreasing α. For $\gamma\alpha < 1$, we find $D_{a+} \approx \gamma D_+ \equiv D_a$, the usual ambipolar diffusion coefficient without negative ions. For plasmas in which $\alpha \gg 1$ in the centre of the discharge, the entire transition region takes place over a small range of $1/\gamma < \alpha < 1$ near the edge of the electronegative region, such that the simpler value of

$$D_{a+} = 2D_+ \tag{2.15}$$

holds over most of the electronegative region.

Using (2.12), the steady-state positive ion continuity equation $\nabla\cdot\Gamma_i = G_i - L_i$ is

$$-\frac{\mathrm{d}}{\mathrm{d}x}\left(D_{a+}(\alpha)\frac{\mathrm{d}n_+}{\mathrm{d}x}\right) = K_{iz}n_g n_e - K_{rec}n_+n_-. \tag{2.16}$$

Within the electronegative region, we can substitute for n_e and n_- using the Boltzmann relations relating electron and ion densities $(n_e/n_{e0}) = (n_-/n_{-0})^{1/\gamma}$ and the plasma approximation of charge neutrality $n_+ = n_- + n_e$ to obtain

$$n_+ = n_- + n_{e0}\left(\frac{n_-}{n_{-0}}\right)^{1/\gamma}. \tag{2.17}$$

Because $\gamma \gg 1$ as a consequence of our assumption of Boltzmann negative ions, we see from (2.17) that $n_e \simeq n_{e0}$. Using this in (2.16) and (2.17) results in a relatively simple differential equation in a single variable n_+.

Equation (2.16) (not making the assumption that $n_e \simeq n_{e0}$) has as a boundary condition at the sheath edge, $x = \ell_p$, that the ion flow cannot exceed the local ion sound velocity, which at the plasma edge is the Bohm velocity. Stating this condition as an equality, it becomes the Bohm flux condition

$$-D_{a+}\left.\frac{\mathrm{d}n_+}{\mathrm{d}x}\right|_{x=\ell_p} = n_+(\ell_p)u_B(T_e, T_i, \alpha_s). \tag{2.18}$$

Here $\alpha_s = \alpha(\ell_p) = n_-(\ell_p)/n_e(\ell_p)$. Since negative ions may be present when (2.18) is satisfied, the Bohm velocity has the general form [20]

$$u_B = \left[\frac{eT_e(1+\alpha_s)}{M_+(1+\gamma\alpha_s)}\right]^{1/2} \tag{2.19}$$

which reduces to the usual expression $u_{B0} = (eT_e/M_+)^{1/2}$ when $\alpha_s = 0$. For $\alpha_s > 1/\gamma$, the negative ion density at the sheath edge significantly reduces the Bohm velocity.

2.2. Conservation equations

Equation (2.16) can be used to determine three parameters: $\alpha_0 = n_{-0}/n_{e0}$ (the ratio of n_- to n_e at the plasma centre), n_{e0}, and T_e. We can determine these by solving (2.16) together with two particle conservation equations, which are integrated forms of (2.6) and (2.7), and as an energy conservation equation. These are: positive ion particle balance,

$$-D_{a+}\left.\frac{\mathrm{d}n_+}{\mathrm{d}x}\right|_{x=\ell_p} = \int_0^{\ell_p} K_{iz}n_g n_e\,\mathrm{d}x - \int_0^{\ell_p} K_{rec}n_+n_-\,\mathrm{d}x \tag{2.20}$$

negative ion particle balance (negligible negative wall flux),

$$\int_0^{\ell_p} K_{att}n_g n_e\,\mathrm{d}x - \int_0^{\ell_p} K_{rec}n_+n_-\,\mathrm{d}x = 0 \tag{2.21}$$

and energy balance for the electrons,

$$S_e = 2e\mathcal{E}_c\int_0^{\ell_p} K_{iz}n_g n_e\,\mathrm{d}x + 2e\mathcal{E}_w n_+(\ell_p)u_B. \tag{2.22}$$

All volume processes in the sheaths are neglected. Here $\mathcal{E}_c(T_e)$ is the collisional energy lost per electron–positive ion pair created, and $\mathcal{E}_w = 2T_e$ is the electron kinetic energy lost to the wall per electron–ion pair lost to the wall. Given the neutral density, n_g, and the power per unit area deposited in the electrons, S_e, the three equations can be simultaneously solved for the three unknowns T_e, α_0, and n_{e0}, provided ℓ_p is known. The plasma half-width ℓ_p differs from the half-length of the device by a sheath width s. In a complete model we must determine s self-consistently with ℓ_p, given the discharge heating mechanism. A common assumption (only marginally satisfied in some capacitive radiofrequency (rf) discharges) is that $s \ll \ell_p$. The set of equations (2.16)–(2.22) can only be solved numerically, since they are nonlinear. In addition, particularly at relatively low pressure and low α,

there is a significant edge region in which the mobility and n_e are not constant, such that the basic equations (2.6) and (2.7) have non-constant coefficients. There is also a fundamental problem in the regions where the negative ions have fallen to very small values, where larger electric fields tend to sweep the negative ions, that are created by attachment, into the electronegative core. As we shall see in the next section, various reasonable approximations allow analytic solutions to be obtained by separating the plasma into a core electronegative region with constant parameters, and an edge electropositive region. Before doing this we explore the range of validity of the various approximations that we have made in this section.

2.3. Validity of reduced equations

We examine the condition for validity of the Boltzmann equilibrium for negative ions, from which we have derived a single ambipolar equation for the positive ions. From (2.1) for negative ions, we have

$$\Gamma_- = -D_- \frac{\mathrm{d}n_-}{\mathrm{d}x} - n_- \mu_- E \tag{2.23}$$

with the condition for Boltzmann equilibrium being that

$$\left| \Gamma_- / D_- \frac{\mathrm{d}n_-}{\mathrm{d}x} \right| \ll 1 \tag{2.24}$$

everywhere. Using the integral relation between the source and the flux, Γ_- can be written as

$$\Gamma_- = \int_0^x K_{att} n_g n_e \,\mathrm{d}x - \int_0^x K_{rec} n_+ n_- \,\mathrm{d}x. \tag{2.25}$$

If we have profiles for n_e, n_-, and n_+, (2.25) can be explicitly evaluated, as we shall do in the next section. Since the recombination increases with the square of the density, at high density (2.24) is no longer satisfied. We can estimate the left-hand side of (2.24) using (2.25) and the solution which holds where (2.24) is satisfied. We have done this in [17], finding a parabolic solution for which (2.24) has its maximum value at $x = 0$, giving the condition for which negative ions in the electronegative plasma are in Boltzmann equilibrium, i.e. satisfies (2.24),

$$\rho \equiv \frac{7}{30} K_{rec} n_{e0} \alpha_0 \ell_p^2 / D_- < 1. \tag{2.26}$$

Since in (2.26) we have taken the largest value that (2.24) attains, we have used a simple rather than a strong inequality in (2.26).

If (2.26) is not satisfied, the negative ions are not in Boltzmann equilibrium and (2.16) is not valid, but the electron profile may still be quite flat, which also allows the reduction to a single differential equation for the profile. Using (2.23) and (2.25) beyond this transition, but taking $n_e = n_{e0}$, we have

$$n_- \mu_- E(x) = -\left(\int_0^x K_{att} n_g n_{e0} \,\mathrm{d}x - \int_0^x K_{rec} n_+ n_- \,\mathrm{d}x + D_- \frac{\mathrm{d}n_-}{\mathrm{d}x} \right). \tag{2.27}$$

The electric field is now determined implicitly in terms of integrals over the source terms, plus a usually small gradient correction. Because $T_e \gg T_i$, there is a large parameter range in which (2.26) is not satisfied but n_e is still essentiality flat, as determined by the Boltzmann relation. To determine this condition, explicitly, we first assume that all terms involving variation of n_e are negligible. Then we can substitute (2.27) into (2.6) and, using the approximations that $n_- \simeq n_+$ ($n_e \ll n_-$), $\mu_- = \mu_+$, $T_- = T_+$, and dropping small terms, we obtain

$$\frac{\mathrm{d}}{\mathrm{d}x}\left[-2D_+ \frac{\mathrm{d}n_+}{\mathrm{d}x} + \int_0^x K_{rec} n_+^2 \,\mathrm{d}x - \int_0^x K_{att} n_g n_{e0} \,\mathrm{d}x \right] \approx K_{iz} n_g n_{e0} - K_{rec} n_+^2. \tag{2.28}$$

We evaluate the left-hand side to obtain

$$2D_+ \frac{\mathrm{d}^2 n_+}{\mathrm{d}x^2} + (K_{iz} + K_{att}) n_g n_{e0} - 2K_{rec} n_+^2 = 0. \tag{2.29}$$

Equation (2.29) has an elliptic integral solution.

To determine the condition for (2.29) to be valid, we add (2.8) and (2.9). Dropping small terms, we obtain

$$\frac{\mathrm{d}}{\mathrm{d}x}\left(-2D_+ \frac{\mathrm{d}n_-}{\mathrm{d}x} - \gamma D_+ \frac{\mathrm{d}n_e}{\mathrm{d}x} \right) = (K_{iz} + K_{att}) n_g n_e - 2K_{rec} n_+^2 \tag{2.30}$$

where we have used the Einstein relation to write $\mu_+ D_e / \mu_e = \gamma D_+$. Equation (2.30) still is a function of two variables n_e and n_-, so that a simplified form of (2.8) or (2.9) is required to be solved simultaneously with (2.30) to obtain a general solution. Comparing (2.30) with (2.29), we see that (2.29) is just the approximation that the electron gradient term in (2.30) can be dropped, i.e. $n_e^{-1}(\mathrm{d}n_e/\mathrm{d}x) < 2\alpha_0/\ell_p\gamma$. From (2.30) we would expect that, with increasing ρ, at sufficiently high pressure and α_0, the ionization and attachment are increasingly balanced locally by the recombination. In this regime the left-hand side is a perturbation to the right-hand side; the right-hand side by itself gives the proportionality $n_e \propto n_-^2$, which is quite different from the parameters for which $n_e \simeq n_{e0}$, a constant, with n_- varying with position. However, in this regime both n_e and n_- only vary weakly over the main part of the electronegative discharge region.

Using the same procedure that we employed to obtain (2.26), for the validity of a parabolic solution, we can also obtain the condition for validity of the elliptic solution. This is more difficult, since we need to expand the elliptic solution at the origin, and, unlike the parabolic solution, the gradient for the elliptic solution is much flatter and varies greatly with changing parameters. The result, obtained in Lichtenberg *et al* [17], is

$$\kappa \equiv \frac{1}{11.55\alpha_0} \left(\frac{D_+}{K_{rec} n_{e0} \alpha_0 \ell_p^2} \right)^{1/2} \times \exp\left(\frac{2K_{rec} n_{e0} \alpha_0 \ell_p^2}{D_+} \right)^{1/2} < 1. \tag{2.31}$$

The exponential dependence with increasing recombination is the result of the flattening of the elliptic solution with increasing recombination.

3. Models for the principal parameter regimes

Various models can be constructed that approximate the plasma profiles in different regions of the parameter space. As described in the introduction, we make the assumptions that the plasma can be considered one dimensional, with the variation in the axial dimension, and that only one positive ion species is important. These assumptions are often approximately satisfied, and coincide with a series of papers on electronegative equilibria that we draw upon [15–17]. We introduce the regimes and their models here, and then in section 4 construct the equations from which the transitions between the models are obtained. The characterization of the regimes will become more precise in section 4, when the transitions are defined, and in section 5 where scaling laws are found.

3.1. Regime (1), low pressure, moderately high n_{e0} (moderate α_0)

In [15] we used the assumption that the plasma would separate into an electronegative core and an electropositive edge. In the electronegative core we found that if the local recombination between negative and positive ions was everywhere small compared to the gradient of the positive ion ambipolar diffusion flux, if the ambipolar diffusion coefficient can be taken to be constant, and if the electron density is essentially a constant within the electronegative region, then from (2.16) the negative ion density within the core can be approximated by a parabola having a scale length ℓ which goes smoothly to zero at the edge ℓ_- of the electronegative region ($\ell = \ell_-$):

$$\frac{n_+}{n_{e0}} = \frac{n_-}{n_{e0}} + 1 = \alpha_0\left(1 - \frac{x^2}{\ell^2}\right) + 1. \tag{3.1}$$

If (3.1) is substituted into the conservation equations (2.20) and (2.21) for positive ion and negative ion particle balance, we obtain

$$K_{iz} n_g \ell = K_{rec} n_{e0}\left(\frac{8}{15}\alpha_0^2 + \frac{2}{3}\alpha_0\right)\ell + \frac{2\bar{D}_a + \alpha_0}{l} \tag{3.2}$$

$$K_{att} n_g \ell_p = K_{rec} n_{e0}\left(\frac{8}{15}\alpha_0^2 + \frac{2}{3}\alpha_0\right)\ell \tag{3.3}$$

where $\bar{D}_{a^+}$ is obtained by using an α, averaged over a parabolic profile

$$\bar{D}_{a^+} = D_+ \frac{1 + \gamma + 2\gamma\bar{\alpha}}{1 + \gamma\bar{\alpha}} \tag{3.4}$$

where $\bar{\alpha} = \frac{2}{3}\alpha_0$.

In the electropositive edge region the positive ion particle balance can be approximated as [16]

$$\frac{2\bar{D}_{a^+}\alpha_0}{\ell} + K_{iz} n_g(\ell_p - \ell) = h_l u_{B0}. \tag{3.5}$$

For simplicity we take $n_e = n_{e0}$ in this edge region for calculating the ionization, $u_{B0} = (eT_e/M_+)^{1/2}$, and $h_l = n_s/n_{e0}$, which is given at low pressures by [16]

$$h_l = \left[\frac{a + (u(\ell)/u_{B0})^3}{1 + a}\right]^{1/3} \tag{3.6}$$

where n_s is the electron (and positive ion) density at the plasma-sheath edge, $u(\ell)$ is the positive ion velocity at the edge of the electronegative region, and $a = 2\nu_{iz}\lambda/\pi u_{B0}$, with $\nu_{iz} = K_{iz} n_g$ and λ is the ion mean free path. For a given feedstock gas, if n_g, n_{e0} and ℓ_p are known, the unknown quantities α_0, ℓ, and T_e can be determined from the above equations.

3.2. Regime (2), low pressure, moderately low n_{e0} (moderately high α_0)

Depending on plasma parameters, it is possible for ions to attain the local ion sound velocity in the electronegative region. In this case, if we use the parabolic approximation for negative ions, the electronegative region terminates abruptly at a position $\ell_- < \ell$, where an internal non-neutral transition region forms [16]. the particle balance equation for positive ions is then

$$K_{iz} n_g n_{e0} \ell_- = K_{rec} n_{e0}^2\left[\alpha_0^2 \ell_-\left(1 - \frac{2}{3}\frac{\ell_-^2}{l^2} + \frac{1}{5}\frac{\ell_-^4}{l^4}\right) + \alpha_0 \ell_-\left(1 - \frac{1}{3}\frac{\ell_-^2}{\ell^2}\right)\right] + n_{e0}\left[\alpha_0\left(1 - \frac{\ell_-^2}{\ell^2}\right) + 1\right] u_B(\alpha_-) \tag{3.7}$$

where

$$u_B(\alpha_-) = \left(\frac{eT_i}{M_+}\frac{\alpha_- + 1}{\alpha_- + 1/\gamma}\right)^{1/2} \tag{3.8}$$

with

$$\alpha_- = \alpha_0(1 - \ell_-^2/l^2) \tag{3.9}$$

and equations (3.3) and (3.5) are modified accordingly. Since $\ell \neq \ell_-$, we have an additional parameter which requires an additional equation, which is that the local sound speed is attained within the electronegative region [16]

$$\frac{2\bar{D}_{\alpha^+}\alpha_0 n_{e0}\ell_-}{\ell^2} = \left[\alpha_0\left(1 - \frac{\ell_-^2}{\ell^2}\right) + 1\right] n_{e0} u_B(\alpha_-). \tag{3.10}$$

Approximating $u_B(\alpha_-)$ from (3.8) as

$$u_B(\alpha_-) = v_{th}\left(\frac{1 + \alpha_-}{\alpha_-}\right)^{1/2} \tag{3.11}$$

where $v_{th} = (eT_i/M_+)^{1/2}$, then (3.10) yields a cubic equation for ℓ_-^2/ℓ^2:

$$\left(\frac{4\lambda}{\ell}\right)^2 \alpha_0^3 \frac{\ell_-^2}{\ell^2}\left(1 - \frac{\ell_-^2}{\ell^2}\right) = \left[1 + \alpha_0\left(1 - \frac{\ell_-^2}{\ell^2}\right)\right]^3. \tag{3.12}$$

Equation (3.12) yields solutions for sufficiently low pressure and low n_{e0}; otherwise the local ion sound speed is not attained in the electronegative region and $\ell = \ell_-$.

3.3. Regime (3), high pressure, moderately high n_{e0} (moderately high α_0)

At higher pressures the parabolic solution does not adequately describe the solution to the ambipolar diffusion equation. In particular, the recombination of positive and negative ions results in a central flattening of the electronegative discharge profile and a steepening of the edge

electronegative region. Provided the ion sound limit is not reached, the electronegative core profile can be approximated by [17]

$$n_+ \simeq n_- = \alpha_0 n_{e0} \qquad 0 < x < \ell_- - d$$
$$n_+ \simeq n_- = \alpha_0 n_{e0}\left(1 - \frac{(x+d-\ell_-)^2}{d^2}\right)$$
$$\ell_- - d < x < \ell_- \tag{3.13}$$

which is flat-topped with parabolic edge regions. Substituting (3.,13) into the basic equations (2.20) and (2.21) and using a modified (3.5), we eliminate K_{iz} to obtain

$$K_{att} n_g \ell_p = K_{rec}\alpha_0^2 n_{e0}\ell_- \tfrac{7}{15} K_{rec}\alpha_0^2 n_{e0} d \tag{3.14}$$

and

$$\left(K_{att} n_g + \frac{h_l u_{B0}}{\ell_p}\right)\ell_- - K_{att} n_g \ell_p = 4D_+\frac{\alpha_0}{d}. \tag{3.15}$$

The additional equation for the parameter d (size of the varying part of the electronegative region having a strong density gradient) is found from the condition that the electric field-driven negative ion mobility flux must balance the negative ion diffusion flux in the strong gradient region to make $\Gamma_-(\ell_-) = 0$ [17], which leads to (with $D_+ = D_-$)

$$2D_+\alpha_0 n_{e0}/d = \tfrac{7}{15} K_{rec} n_{e0}^2 \alpha_0^2 d. \tag{3.16}$$

From (3.14) with $d \ll \ell_-$ ($\ell_- \simeq \ell_p$), α_0 is approximated as

$$\alpha_0 \simeq \left(\frac{K_{att} n_g}{K_{rec} n_{e0}}\right)^{1/2} \tag{3.17}$$

and using the high α_0 approximation for h_l in (3.6)

$$h_l \simeq \frac{u(\ell)}{u_{B0}} = \frac{4D_+\alpha_0}{d u_{B0}}. \tag{3.18}$$

We can readily solve (3.15) and (3.16) for the remaining parameters d and ℓ_-. At higher pressures if $\lambda/(\ell_p - \ell_-) < T_i/T_e$, the value of h_l, determined by the high-pressure diffusion solution in the electropositive edge, is somewhat different than the low-pressure value given by (3.6) [15]. We have retained (3.6) in order to have a smooth transition when $d = \ell_-$.

3.4. Regime (4), high pressure, moderate n_{e0} (high α_0)

The ion sound velocity can also be reached in the higher pressure region due to the steepening of the electronegative edge gradients. In this case the scale length d in the denominator of (3.13) is replaced by ℓ, $\ell \neq d$, and the equilibrium equations are modified accordingly, with (3.12) in the ℓ_- is replaced with d supplying the additional equation.

3.5. Regimes (5) and (6), low and high pressure, low n_{e0} (high α_0)

In both the low- and high-pressure regimes there is a transition with decreasing n_{e0} (increasing α_0) to a regime in which an electropositive edge region no longer exists. For these parts of parameter space $\ell_- = \ell_p$, such that, after eliminating the terms in K_{iz}, (3.10) reduces to

$$2\bar{D}_{a^+}\alpha_0\ell_p/\ell^2 = u_B(\alpha_-)(\alpha_- + 1) \tag{3.19}$$

with α_- given by (3.9). Since $\ell_- = \ell_p$, the number of variables is reduced by one, as is the number of independent equations.

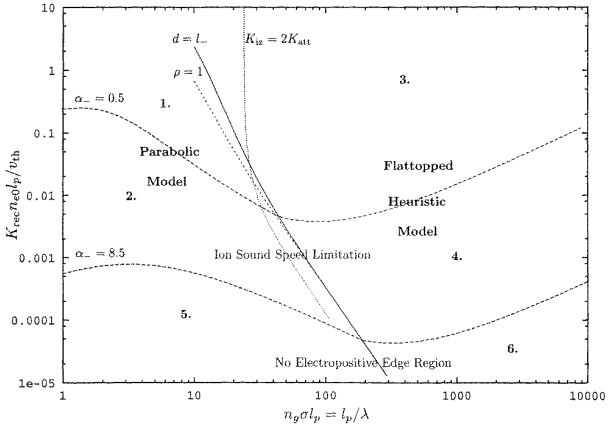

Figure 1. Parameter space of normalized electron density n_{e0} (ordinate) versus normalized gas density n_g (abscissa), for oxygen, showing regions where the various models apply. At constant pressure (gas density) $\alpha_0 \equiv n_{-0}/n_{e0}$ increases with decreasing n_{e0}. At constant n_{e0}, α_0 increases with increasing pressure.

4. Transitions between regimes

An examination of the algebraic equations (3.2)–(3.6), describing the low-pressure moderate α_0 parameter regime (1), shows that there are only two significant independent parameters $n_g\ell_p$ and $n_{e0}\ell_p$, i.e. ℓ_p does not appear separately. Furthermore, if we assume that T_e is essentially clamped due to the exponential dependence of K_{iz} on T_e, then the reduced variable space can be explored using normalized parameters which are conveniently written in non-dimensional form as $\sigma n_g \ell_p = \ell_p/\lambda$ and $K_{rec} n_{e0}\ell_p/v_{th}$, where $v_{th} = (eT_i/M)^{1/2}$ is the ion thermal velocity, assumed given, and σ is the ion momentum cross section. All reaction rates are taken to be fixed characteristics of a given gas at a fixed T_e. The various regimes (1)–(6) for this classification scheme are shown in figure 1. Note that the abscissa is the normalized pressure and the ordinate is the normalized electron density. At low pressure (ℓ_p/λ not too large) we proceed through the transitions from low to high α_0, traversing regimes (1), (2), and (5), when reducing $K_{rec} n_{e0}\ell_p/v_{th}$ (usually reducing n_{e0} for a particular device and feedstock gas). At higher pressure we proceed through the transitions from low to high α_0, traversing regimes (3), (4), and (6), when reducing $K_{rec} n_{e0}\ell_p/v_{th}$.

The transition between the low- and high-pressure regimes is formally obtained from the high-pressure side (regime (3)) by reducing the pressure until the flat central region disappears. At this value of pressure it can be shown [17] that $d = \ell_- = \ell$ (with no ion sound limitation), such that regime (3) joins smoothly to regime (1), as shown in figure 1. However, this does not uniquely determine the transition, since the equations for regime (1) also give solutions in regime (3). We therefore need an additional physical criterion to separate the two regions. We use two such criteria to (roughly) bracket the transition. As mentioned previously, we expect the parabolic solution to be inaccurate when the nonlinear recombination flux (first term on the right-hand side of (3.2) competes with the diffusion flux (second term on the right-hand side of (3.2)). The profile was then shown [17] to be elliptic, rather than parabolic, with a flattening of the

central region. Since attachment balances recombination, from (3.3), this condition of equal fluxes can be simply expressed as

$$K_{iz} = 2K_{att} \tag{4.1}$$

which is shown in figure 1. Another criterion for the breakdown of the parabolic solution is that the ambipolar diffusion solution does not hold, because recombination is sufficient to prevent the negative ions from attaining Boltzmann equilibrium. This transition, assuming a parabolic solution, occurs approximately at [17]

$$\rho \equiv \tfrac{7}{30} K_{rec} n_{e0} \alpha_0 \ell_p^2 / D_- = 1 \tag{4.2}$$

where D_- is the negative ion diffusion coefficient taken here to be equal to D_+. This condition is also plotted in figure 1.

The curves in figure 1 show the transitions and regimes explicitly for oxygen, using the following values of the reaction rate coefficients (see [15])

$$K_{iz} = 2.13 \times 10^{-14} \exp(-14.5/T_e) \text{ m}^3 \text{ s}^{-1} \tag{4.3}$$

$$K_{att} = 7.89 \times 10^{-17} \exp(-3.07/T_e) \text{ m}^3 \text{ s}^{-1} \tag{4.4}$$

$$K_{rec} = 1.4 \times 10^{-13} \text{ m}^3 \text{ s}^{-1} \tag{4.5}$$

$$K_{cx} = 3.95 \times 10^{-16} \text{ m}^3 \text{ s}^{-1} \tag{4.6}$$

where K_{cx}, the charge exchange reaction rate, is the dominant term for determining the cross section, $\sigma = K_{cx}/v_{th}$. The electron temperature, using various analytic and particle-in-cell (PIC) solutions, is nominally taken to be $T_e = 2.5$ eV. We see that the transition curve $d = \ell_-$ lies quite close to the transition $\rho = 1$, strengthening the proposition that we can use the $d = \ell_-$ transition to separate the flat-topped from the parabolic solution. The $K_{iz} = 2K_{att}$ transition, occurring at somewhat higher pressures, indicates that either solution should be a reasonable approximation within this region of parameter space.

Equation (3.12), which gives the value of ℓ_-/ℓ at which the ion sound speed is reached, is found to have, at a given pressure, no real roots for small α_0, and two positive real roots for larger α_0, with the smaller root giving the value of ℓ_-/ℓ [16]. At the transition there is a double root for ℓ_-/ℓ. We find numerically that for all pressures this corresponds approximately to $\alpha_- = 0.5$. Using this value, the transitions between regimes (1) and (2) and between regimes (3) and (4) are readily calculated, as indicated on figure 1.

The transition from regime (2) to regime (5) at which the electropositive region disappears is easily obtained by setting the flux leaving the electronegative plasma equal to the Bohm flux out of the electropositive region

$$n_{e0}(1 + \alpha_-) u_B(\alpha_-) = n_{e0} u_{B0}. \tag{4.7}$$

using (3.11) for $u_B(\alpha_-)$, we obtain

$$(1 + \alpha_-) \left(\frac{1 + \alpha_-}{\alpha_-} \right)^{1/2} = \left(\frac{T_e}{T_i} \right)^{1/2}. \tag{4.8}$$

Substituting a value of $\gamma = T_e/T_i = 100$ into (4.8) we obtain $\alpha_- = 8.5$. Using this value of α_- in the complete set of equations in either regime (2) or (5), we obtain the transition between them shown in figure 1. Equation (4.8) also holds at the transition between regimes (4) and (6).

Although the transitions between the various regions must be obtained by solving the equations, as done in this section, it is possible to get some additional insight into the transitions. In particular, the rather odd form of the transition between regions (1) and (2), and between regions (3) and (4) can be understood from dimensional analysis, which we present in appendix A. The analysis indicates that in the low-pressure regions a rough scaling of $v_D \propto (n_{e0} n_g)^{1/2}$ holds, while in the high-pressure regions the scaling is $v_D \propto (n_{e0}/n_g)^{1/4}$ since the transition occurs for $v_D \gtrsim v_{th}$, where v_{th} is held constant; the transition should have $n_{e0} \propto n_g^{-1}$ in the low pressure region and $n_{e0} \propto n_g$ in the high pressure region. These proportionalities are seen to hold, approximately, for parameters away from the transition between the two pressure regions (on the left-hand edge of figure 1 other factors have become important).

In obtaining figure 1 we have assumed an oxygen plasma with the ions at room temperature. These transitions can be different for other gases. Even for oxygen, a modification occurs if the negative ions are significantly heated. From PIC simulations, in some examples, the negative ions have been found to be at an elevated temperature, with $T_- \simeq 3T_+$. For this case the diffusion coefficient for moderate to large α_0 becomes $D_{a+} = D_+(1 + T_-/T_+) = 4D_+$, which is a factor of two larger than the previously assumed D_{a+}. Since D_{a+} is inversely proportional to the gas density n_g, this means that all numerical results will effectively relate to a density a factor of two lower in the D_{a+} terms. For a feedstock gas such as chlorine, the numerical; shifts are much larger. Chlorine has an attachment reaction rate coefficient approximately a factor of ten larger than oxygen. This shifts the low-to-high pressure solution by approximately a factor of ten towards lower pressure. Because of the α_0 scaling it also strongly raises the transition at which an ion sound limitation appears and the transition at which the electropositive region disappears. In previous oxygen examples we were interested in regimes (1) and (2) [15, 16], while for chlorine regime (6) was of primary interest [8, 17].

In this study we do not treat the regimes at very high pressure, $\kappa > 1$, in (2.31) where the electron density cannot be taken to be constant, or at low pressure where the constant mobility assumption can fail. We also do not consider the scaling for low α_0 ($\alpha_0 < 1$), where some terms become important that were assumed to be small in this work. These restrictions somewhat limit the range of validity of figure 1. For example, although the abscissa of normalized pressure has been taken to large values in the figure, the failure of the constant electron density assumption reduces the accuracy of the last decade. We return to these limitations in section 5.

5. Scaling laws

Scaling laws are useful to determine the plasma behaviour near some known solution. As described in the introduction, approximate scaling laws are obtained from global models (volume-averaged over assumed electropositive and electronegative profiles). These models are most accurate where internal ion loss processes dominate over the flux to the

walls (regimes (3), (4), and (6)) or when the electropositive edge has disappeared (regimes (5) and (6)). In regime (1), which is furthest from the regime covered by global models, fairly precise scaling laws can be uncovered using the results of section 4. Although not large in parameter space, this regime is physically very important, as it encompasses low pressures and high densities, which are very useful for plasma processing. We shall consider this regime in considerable detail, and the other regimes more briefly. In all of the scaling analysis we employ the implicit assumption that the exponentially strong dependence of K_{iz} on T_e essentially clamps the temperature on all other equations.

5.1. Regime (1), low pressure, moderately high n_{e0} (moderate α_0)

Using (3.3)–(3.5) we eliminate the temperature sensitive reaction rate K_{iz} to solve for α_0 and ℓ/ℓ_p (here $\ell = \ell_-$), with an approximate assumed temperature. Furthermore, as noted previously, ℓ_p only appears in the product forms $N_g = n_g\ell_p$ and $N_{e0} = n_{e0}\ell_p$. Then α_0 and ℓ/ℓ_p can be written, from the resulting two equations, in the convenient forms [15]

$$\alpha_0 = -\frac{5}{8} + \left[\left(\frac{5}{8}\right)^2 + \frac{15}{8}\frac{K_{att}}{K_{rec}}\frac{N_g}{N_{e0}}\frac{\ell_p}{\ell}\right]^{1/2} \tag{5.1}$$

and

$$\frac{\ell}{\ell_p} = \{K_{att}N_g + [(K_{att}N_g)^2 + (8v_{th}\alpha_0 f(\alpha_0)/\sigma N_g) \times (h_l u_{B0} + K_{att}N_g)]^{1/2}\}[2(h_l u_{B0} + K_{att}N_g)]^{-1} \tag{5.2}$$

where $f(\alpha_0) = \bar{D}_{a+}/D_+$ is the α_0-dependence of the diffusion in (3.4). For $\alpha_0 \gg \frac{5}{8}$, (5.1) reduces to

$$\alpha_0 \approx \left(\frac{15}{8}\frac{K_{att}}{K_{rec}}\frac{N_g}{N_{e0}}\frac{\ell_p}{\ell}\right)^{1/2} \tag{5.3}$$

and for

$$K_{att}N_g \ll h_l u_{B0} \tag{5.4}$$

but keeping $\alpha_0 \gg \frac{5}{8}$ such that, from (3.4), $f(\alpha_0) = 2$, (5.2) reduces to

$$\frac{\ell}{\ell_p} \approx \left[\frac{4v_{th}\alpha_0}{h_l u_{B0}\sigma N_g}\right]^{1/2} \tag{5.5}$$

with $\lambda = (n_g\sigma)^{-1}$. The relations (5.3) and (5.5) are still coupled and, furthermore h_l, from (3.6) is

$$h_l = \left[\frac{2K_{iz}/\pi\sigma u_{B0} + (u(\ell)/u_{B0})^3}{1 + 2K_{iz}/\pi\sigma u_{B0}}\right]^{1/3} \tag{5.6}$$

which is a complicated function of parameters and also depends sensitively on temperature through K_{iz}. We do not have explicit scaling in (5.3) or (5.5) because h_l in (5.6) has two terms. There is an intermediate transition for

$$(u(\ell)/u_{B0})^3 = a \equiv 2K_{iz}/\pi\sigma u_{B0}. \tag{5.7}$$

For relatively small α_0 with ℓ/ℓ_p significantly less than unity, we use the approximation $a \gg (u(\ell)/u_{B0})^2$. Then h_l can be approximated by

$$h_l \simeq a^{1/3} \simeq (2\lambda/\pi\ell_p) = (2/\pi\sigma N_g)^{1/2}. \tag{5.8}$$

The second approximate equality is obtained from a self-consistent analysis in the low α_0 regime (see appendix B). Substituting (5.8) into (5.5) and solving (5.3) and (5.5) together, we obtain the following proportionalities:

$$\alpha_0 = \left(\frac{15}{8}\frac{K_{att}}{K_{rec}}\frac{N_g}{N_{e0}}\right)^{2/5}\left(\frac{1}{4}\frac{u_{B0}}{v_{th}}\right)^{1/5}(\sigma N_g)^{1/10} \propto (p\ell_p)^{1/2}(n_{e0}\ell_p)^{-2/5} \tag{5.9}$$

and

$$\ell/\ell_p \simeq \left(\frac{v_{th}}{u_{B0}}\right)^{2/5}\frac{1}{(\sigma N_g)^{1/5}}\left(\frac{15}{8}\frac{K_{att}}{K_{rec}}\frac{N_g}{N_{e0}}\right)^{1/5} \propto (n_{e0}\ell_p)^{-1/5}. \tag{5.10}$$

The ℓ/ℓ_p scaling with parameters is very weak and can often be neglected.

Approximation (5.8) is not valid near the transition from regime (1) to regime (3), since for $\ell/\ell_p \sim 1$ the flux into the electropositive region is much larger than the flux generated in that region. There, from (5.6), the approximation

$$h_l \simeq u(\ell)/u_{B0} \tag{5.11}$$

holds, where

$$u(\ell) = \frac{4v_{th}}{\sigma N_g}\frac{\ell_p}{\ell}\alpha_0. \tag{5.12}$$

Substituting (5.11) and (5.12) into (5.5) we find that $\ell/\ell_p \sim 1$. using this result in (5.3) we find, near the transition between regimes (1) and (3),

$$\alpha_0 \simeq \left(\frac{15}{8}\frac{K_{att}}{K_{rec}}\frac{N_g}{N_{e0}}\right)^{1/2} \propto \left(\frac{p\ell_p}{n_{e0}\ell_p}\right)^{1/2} \tag{5.13}$$

which is independent of ℓ_p. This square root scaling essentially holds over all of the other regimes, except that the numerical factor of $(15/8)^{1/2}$ slowly becomes unity as the parameters change towards lower n_{e0} and higher n_g.

An important physical parameter is the wall flux Γ_{+w}. Normalizing this to $n_{e0}u_{B0}$, which is useful in regimes (1)–(4), we have

$$\Gamma_{+w(norm)} = h_l. \tag{5.14}$$

As discussed above, from (5.6) h_l divides into two regions. For smaller α_0, h_l is given by (5.8), which when substituted in (5.14) gives

$$\Gamma_{+w(norm)} = \left(\frac{2}{\pi\sigma N_g}\right)^{1/2} \propto (p\ell_p)^{-1/2}. \tag{5.15}$$

For higher α_0, we substitute (5.11), (5.12), and (5.34) with $\ell_p/\ell \simeq 1$ in (5.14) to obtain

$$\Gamma_{+w(norm)} = \left(\frac{15}{8}\frac{K_{att}N_g}{K_{rec}N_{e0}}\right)^{1/2}\frac{4v_{th}}{u_{B0}\sigma N_g} \propto (p\ell_p)^{-1/2}(n_{e0}\ell_p)^{-1/2} \tag{5.16}$$

with has the same $p\ell_p$ scaling as (5.15).

Comparing $\Gamma_{+w(norm)}$ in (5.15) and (5.16) with the scaling of α_0 in (5.9) and (5.13), we see that the $p\ell_p$ scalings are inverse to one another.

5.2. Regime (2), low pressure, moderate n_{e0} (moderately high α_0)

The scaling of α_0 is approximately that given by (5.3) with $\ell/\ell_p \simeq$ constant ~ 1. for Γ_{+w} we evaluate $\Gamma_+(\ell_-)$ at $\ell_- = \ell_p$ to obtain

$$\Gamma_{+w(norm)} = 4\frac{v_{th}}{u_{B0}}\frac{\lambda}{\ell_p}\frac{\ell_p}{\ell}\alpha_0. \tag{5.17}$$

Again ignoring the weak ℓ_p/ℓ scaling we have

$$\Gamma_{+w(norm)} \propto (p\ell_p)^{-1/2}(n_{e0}\ell_p)^{-1/2} \tag{5.18}$$

which is the same as in regime (1).

5.3. Regime (3), high pressure, moderately high n_{e0} (moderate α_0)

Here we again use the global scaling of α_0 which is valid at high pressures as given in (3.17), with $D_+ = v_{th}\lambda$,

$$\frac{d}{\ell_p} = \left(\frac{30}{7}\right)^{1/2}\left(\frac{v_{th}\lambda}{K_{rec}\alpha_0 n_{e0}}\right)^{1/2}\frac{1}{\ell_p} = \frac{(\frac{30}{7}v_{th}\lambda)^{1/2}/\ell_p^{1/2}}{(K_{rec}N_{e0}K_{att}N_g)^{1/4}}$$
$$\propto (p\ell_p)^{-3/4}(n_{e0}\ell_p)^{-1/4}. \tag{5.19}$$

Substituting (5.19) into (5.17) with d replacing ℓ,

$$\Gamma_{+w(norm)} = \frac{(\frac{56}{15}v_{th}\lambda/\ell_p)^{1/2}(K_{att}N_g)^{3/4}}{u_{B0}(K_{rec}N_{e0})^{1/4}} \propto \frac{(p\ell_p)^{1/4}}{(n_{e0}\ell_p)^{-1/4}} \tag{5.20}$$

we find that the h_l dependence is very weak and independent of ℓ_p.

5.4. Regime (6), high pressure, low n_{e0} (high α_0)

Regime (5) is generally unimportant. Regimes (4) and (6) can be quite important for strongly attaching gases, such as chlorine, which are also often used in applications at higher pressure [8]. As seen in section 3, the equations become quite complicated. However, the important scalings are not too different from regime (3). We have already considered this regime, for chlorine feedstock gas, using various approximations and models in [17].

5.5. Transition from wall to recombination dominated loss

We can also find the scaling of the transition between the wall flux dominated regime and the recombination dominated regime. Noting, as previously, that the recombination flux is equal to the attachment, we have

$$R_L = \frac{\Gamma_{rec}}{\Gamma_+(\ell_p)} = \frac{K_{att}N_g}{h_l u_{B0}} = 1 \tag{5.21}$$

which is equivalent to the condition $K_{iz} = 2K_{att}$ in figure 1. Substituting for h_l from (3.18) with d/ℓ_p given by (5.19) and α_0 given by (3.17), we obtain

$$R_L = \frac{15}{56}\left(\frac{\sigma N_g}{v_{th}}\right)^{1/2}(K_{att}N_g K_{rec}N_{e0})^{1/4}$$
$$\propto (p\ell_p)^{3/4}(n_{e0}\ell_p)^{1/4}. \tag{5.22}$$

Table 1. Values of α_0 versus p (mTorr) and n_{e0} (cm) for $T_e = 2.5$ eV, $\ell_p = 2$ cm.

	p			
	1	10	100	1000
$n_{e0} = 10^{10}$				
ℓ_p/λ	0.67	6.7	67	670
α_0	0.95	3	6.9	21.9
	n_{e0}			
	10^{11}	10^{10}	10^9	10^8
$p = 10$				
$K_{rec}n_{e0}\ell_p/v_{th}$	0.7	0.07	0.007	0.0007
α_0	1.1	3	7.5	23.7

5.6. Illustrating the boundaries and scalings

Consider as a base case a practical configuration that has been simulated by a PIC code of an O_2 feedstock capacitive discharge between plates of 6 cm spacing [15]. The high voltage across the discharge gave sheaths of approximately 1 cm, such that the plasma half-width can be taken to be $\ell_p = 2$ cm. The simulation was performed at a pressure $p = 10$ mTorr ($n_g = 3.2 \times 10^{14}$ cm^{-3}) and an electron density $n_{e0} = 10^{10}$ cm^{-3}. First, taking a nominal $T_e = 2.5$ eV, corresponding to our oxygen discharge of figure 1, we calculate from (4.3) and (4.4) the reaction rates $K_{iz} \simeq 6.4\times10^{-17}$ m^3 s^{-1} and $K_{att} = 2.3\times10^{-17}$ m^3 s^{-1}. Using the value of K_{att}, the values of K_{rec} and K_{cx} from (4.5) and (4.6) and taking $v_{th} = 3.9 \times 10^4$ cm s^{-1}(1/40 eV), we calculate α_0 from (5.9) for the base case, obtaining $\alpha_0 = 3$. The normalized coordinates are $\ell_p/\lambda = 6.7$ and $K_{rec}n_{e0}\ell_p/v_{th} = 0.07$, putting the base case well in the pressure range of the parabolic approximation, and just inside region (1), near the border with region (2), justifying our use of the region (1) formulae. Using the scaling from (5.9) to determine α over a wide range of parameters, we then construct table 1. The gross scaling of $\alpha_0 \propto p^{1/2}n_{e0}^{-2/5}$ is corrected by the crossing of the transition between regions (1) and (3) which eliminates the 15/8 numerical factor from deep within region (1) to deep within region (3). Both the normalized and unnormalized values of the pressure and electron density rate are given to facilitate the understanding of the physical conditions.

In a second illustration of the use of these scalings we take the same base case from the PIC simulation but use the average temperature obtained from that simulation of $T_e \simeq 2$ eV. The distribution is actually bi-Maxwellian with a colder bulk and a hotter tail [15]. We note that this average temperature is different from the nominal temperature used for constructing figure 1. Using $T_e = 2$ eV we find that $K_{att} = 1.8 \times 10^{-17}$ m^3 s^{-1}. Because K_{att} is most sensitive to the bulk distribution which is cooler, it is actually lower than the above value. Using the above values with α_0 given by (5.9) we obtain $\alpha_0 = 2.7$. The value from the PIC simulation is $\alpha_0 = 1.5$ [15]. Recognizing for this small value of α_0 that a correction to the scaling formula is required, we use (5.1) to compute the revised value of $\alpha_0 = 2.24$ to be used in (5.9) for scaling. We did a second PIC simulation, also in region (1), with $\ell_p = 1.2$ cm, $p = 50$ mTorr, and $n_{e0} = 2.5\times10^9$ cm^{-3}. For that case we found $\alpha_0 \simeq 6.8$. Scaling with (5.9)

from $\alpha_0 = 2.24$ we obtain $\alpha_0 = 6.3$, which is in good agreement with the PIC simulation. Thus, judicious use of the scaling formulae, together with a PIC simulation, allows high accuracy without additional simulations.

Although the electron density is a convenient scaling parameter, the power absorbed is the usual control parameter. If we use the total absorbed power as a control parameter we must determine the power absorbed by the ions, as well as by the electrons. This requires a knowledge of the heating mechanisms. Here we shall consider only the power absorbed by the electrons, P_{abse}, which may or may not approximate the total power P_{abs}.

For the regimes of (1), (2) and (5) where $\Gamma_{rec} \ll \Gamma_+(\ell_p)$, the electron absorbed power per unit area is approximately [18]

$$P_{abse} \simeq n_{e0} h_l u_{B0} (\mathcal{E}_c + 2T_e) \tag{5.23}$$

where $\mathcal{E}_c$ is the energy lost per ionization, which depends on K_{iz} as [18]

$$\mathcal{E}_c = \mathcal{E}_{iz} + \frac{K_{exc}}{K_{iz}} \mathcal{E}_{exc}. \tag{5.24}$$

For low pressure with $T_e \gtrsim 2.5$ V, $\mathcal{E}_c$ does not depend sensitively on T_e. Since we are taking T_e to be nearly constant, we also assume $\mathcal{E}_c =$ constant. Substituting for h_l from (5.8) in (5.23), with $T_e \ll \mathcal{E}_c$, we have the scaling

$$n_{e0} \propto P_{abse} (p\ell_p)^{1/2}. \tag{5.25}$$

In the recombination-dominated regimes, (3), (4), and (6), where $\Gamma_{rec} \gg \Gamma_+(\ell_p)$, the power absorbed per unit area can be approximated by

$$P_{abse} \simeq K_{rec} n_+ n_- \ell_p \mathcal{E}_c \tag{5.26}$$

with $n_+ \simeq n_-$, and $K_{rec} =$ constant. This gives

$$n_+ \propto P_{abse}^{1/2} \ell_p^{-1/2} \tag{5.27}$$

and using α_0, from (5.13),

$$n_{e0} \propto P_{abse} (p\ell_p)^{-1}. \tag{5.28}$$

Thus n_{e0} scales the same with P_{abse} in both regimes.

6. Conclusions and discussion

We have reviewed the equilibrium plasma profiles that are obtained in the various regimes in the $n_{e0}\ell_p$–$p\ell_p$ parameter space of an attaching (electronegative) gas. Throughout the analysis the assumptions that the plasma is one dimensional and that the plasma consists of one positive and one negative ion species, in addition to electrons, have been used. The models used divide the space into six regimes. Specifically, using the reaction rates for oxygen, a map of the parameter space has been obtained in terms of the dimensionless parameters $K_{rec} n_{e0} \ell_p / v_{th}$ and ℓ_p/λ. The transition between the low-pressure and high-pressure regimes has been discussed in terms of various criteria, which define a diffuse but relative narrow region of ℓ_p/λ for which the transition takes place.

At low pressure, the electronegative core can be modelled by either a parabola or a truncated parabola, depending on whether the local positive ion velocity does not reach or reaches the local ion sound velocity, respectively. At high pressure the central part of the electronegative core become flattened, but the edges can still be modelled by parabolic regions which have the same type of transition. The key quantity is $\alpha_- \equiv n_-(\ell_-)/n_{e0}$, increasing downward on figure 1, with $\alpha_- \simeq 0.5$ at the transition. For either low or high pressure an additional transition occurs at $\alpha_- = 8.5$, independent of feedstock gas, where the electropositive edge region essentially disappears.

Scalings have been obtained, in some of the more important parameter regimes, giving the dependences of the plasma quantities on the input parameters $p\ell_p$ and $n_{e0}\ell_p$. These are particularly useful in scaling results that have been obtained from time-consuming numerical analysis, such as PIC simulations, to other parameters. The scaling results indicate that many of the important plasma quantities scale similarly across the parameter boundaries, with only small (order unity) changes in the coefficients which connect the plasma quantities to the input quantities. For example, the very important electronegative quantity $\alpha_0 = n_{-0}/n_{e0}$ scales over the entire $p\ell_p$–$n_{e0}\ell_p$ parameter space approximately as $\alpha_0 \propto (p\ell) p^{1/2} (n_{e0}\ell_p)^{-1/2}$, thus allowing reasonable good values of α_0 to be obtained in any part of the space if one value is known.

In applying the models and scalings, discussed in this paper, some care must be exercised in relating the model assumptions to the physical problem. We have already discussed the inaccuracies resulting from using reaction rates based on a Maxwellian electron distribution to compute plasma quantities in situations where the plasma is not Maxwellian. This was the case in the example of a low-pressure PIC simulation for a parallel-plate rf discharge that was used to illustrate the scaling. In that situation the scaling could be used effectively, but the reaction rates had to be adjusted first, on the basis of a point comparison, before the scaling could be used to give accurate results. However, with changes of pressure the distribution function also changes, leading to varying reaction rates at a given average electron temperature. This has been observed experimentally in electropositive plasmas [21], and in PIC simulations of electronegative plasmas [5, 6]. A more complete analysis, including the electron kinetics from which the non-Maxwellian electron distribution has been obtained, has been performed for both electropositive and electronegative plasmas [22].

Other assumptions that must be checked are: having effectively a one-dimensional discharge and having only three charged species. For example, in a discharge with an oxygen feedstock gas, operated at high power, there can be a substantial component of atomic oxygen ions. The existence of such a significant fourth charged component would modify all of the basic equations and consequently all of the analysis. This situation has only been treated within a global analysis in which there are no spatial variations of the species [7]. There are probably interesting possibilities of connecting multi-species global analysis with the three-species, spatially-varying analysis presented here, but they have not yet been explored. All real plasma devices have more than one spatial dimension. The high-aspect-ratio case,

treated here, reasonably well approximates many devices. The other limit, of a long thin device, is also treatable by the types of models considered here, but details have not been worked out. For cylindrical plasma devices with the diameter approximately the same as the axial length, there are certainly differences in the quantitative relations between the plasma quantities and the input parameters. How well the scalings apply is yet to be explored.

Finally, we mention, again, that our models deal only with the equilibrium, rather than the complete discharge. For different types of excitation it is possible to understand a more complete analysis, taking into account sheath widths, ion energy lost in high-voltage sheaths, and other input parameters such as applied voltages. This has been extensively done for electropositive plasmas, including scalings (for a review, see [18, ch 11]). The analysis here can also be connected to the sheath dynamics to completely specify the problem.

Acknowledgments

This work was partially supported by NSF grant ECS-9529658, a gift from the Lam Research Corporation, and the University of California Semiconductor Manufacturing Alliance for Research and Training. One of the authors (THC) acknowledges the financial support from Dong-A University and the Basic Science Research Institute Program, Korea Ministry of Education (BSRI-97-2439). Discussions with Dr R N Franklin are gratefully acknowledged.

Appendix A

We consider the edge scaling

$$v_{Di} = \Gamma_i / n_i \tag{A.1}$$

and require $v_{Di} > v_{th_i}$, where $v_{th_i} =$ constant. From (2.20) with recombination neglected

$$\Gamma_i \propto n_g n_{e0} \ell_p. \tag{A.2}$$

Using (5.3), with $\ell_p/\ell \simeq$ constant, or (3.17) we take

$$\alpha_0 \propto (n_g/n_{e0})^{1/2}$$

and consequently

$$n_i \propto \alpha_0 n_{e0} \propto (n_g n_{e0})^{1/2}. \tag{A.3}$$

Combining (A.1), (A.2), and (A.3),

$$v_D \propto (n_g n_{e0})^{1/2} \tag{A.4}$$

which gives the boundary scaling between regions (1) and (2) of $n_{e0} \propto n_g^{-1}$.

In contrast, at high pressure, there is a near balance between ionization and recombination in the bulk, so that

$$\Gamma_i \propto n_g n_{e0} d \tag{A.5}$$

where d is the edge region thickness given from (3.16) as

$$d \propto n_{e0}^{-1/4} n_g^{-3/4}. \tag{A.6}$$

Substituting (A.3), (A.5), and (A.6) in (A.1) gives

$$v_D \propto (n_{e0}/n_g)^{1/4} \tag{A.7}$$

which gives a boundary between regions (3) and (4) of $n_{e0} \propto n_g$.

Appendix B

Equating ionization to loss when $\Gamma_{+w} \gg \Gamma_{+rec}$,

$$\nu_{iz} n_{e0} \ell_p \simeq u_{B0} h_l n_{e0} \tag{B.1}$$

which for $h_l = a^{1/3}$, from (5.8), gives

$$\nu_{iz} \ell_p \simeq u_{B0} \left(\frac{2\nu_{iz}\lambda_i}{\pi u_{B0}} \right)^{1/3}. \tag{B.2}$$

Rearranging,

$$\nu_{iz}^{2/3} \simeq \frac{u_{B0}^{2/3}}{\ell_p^{2/3}} \left(\frac{2\lambda_i}{\pi \ell_p} \right)^{1/3} \tag{B.3}$$

substituting back into h_l,

$$h_l \simeq \left(\frac{2\lambda_i}{\pi u_{B0} \ell_p} \right)^{1/3} \left(\frac{2\lambda_i}{\pi \ell_p} \right)^{1/6} u_{B0}^{1/3} \tag{B.4}$$

or finally

$$h_l \simeq \left(\frac{2\lambda_i}{\pi \ell_p} \right)^{1/2}. \tag{B.5}$$

References

[1] Edgley P D and Von Engel A 1980 *Proc. R. Soc.* A **370** 375
[2] Park S K and Economou D J 1990 *J. Appl. Phys.* **68** 3904
[3] Sommerer T J and Kushner M J 1992 *J. Vac. Sci. Technol.* B **10** 2179
[4] Chung T H, Meng L, Yoon H J and Lee J K 1997 *Japan. J. Appl. Phys.* **36** 274
[5] Vahedi V and Surendra M 1995 *Comput. Phys. Commun.* **87** 179
[6] Vahedi V 1993 Modeling and simulation of RF discharges used for plasma processing *PhD Thesis* University of California
[7] Lee C, Graves D B, Lieberman M A and Hess D W 1994 *J. Electrochemical Soc.* **141** 6
Lee C and Lieberman M A 1995 *J. Vac. Sci. Technol.* A **13** 368
[8] Lee Y T, Lieberman M A, Lichtenberg A J, Bose F, Baltes H and Patrick R 1997 *J. Vac. Sci. Technol.* A **15** 113
[9] Lieberman M A and Ashida S 1996 *Plasma Sources Sci. Technol.* **5** 145
[10] Ferreira C M, Gousset G and Touzeau M 1988 *J. Phys. D: Appl. Phys.* **21** 1403
Ferreira C M and Gousset G 1991 *J. Phys. D: Appl. Phys.* **24** 775
[11] Tsendin L D 1989 *Sov. Phys.–Tech. Phys.* **34** 11
[12] Kaganovich I D and Tsendin L D 1993 *Plasma Phys. Rep.* **19** 645
[13] Haas F A, Lea L M and Holmes A J T 1991 *J. Phys. D: Appl. Phys.* **24** 1541
[14] Franklin R N, Daniels P G and Snell J 1993 *J. Phys. D: Appl. Phys.* **26** 1638
Franklin R N and Snell J 1994 *J. Phys. D: Appl. Phys.* **27** 2102
[15] Lichtenberg A J, Vahedi V, Lieberman M A and Rognlien T 1994 *J. Appl. Phys.* **75** 2339
[16] Kouznetsov I G, Lichtenberg A J and Lieberman M A 1996 *Plasma Sources Sci. Technol.* **5** 662
[17] Lichtenberg A J, Kouznetsov I G, Lee Y T, Lieberman M A, Kaganovich I D and Tsendin L D 1997 *Plasma Sources Sci. Technol.* **6** 437
[18] Lieberman M A and Lichtenberg A J 1994 *Principles of Plasma Discharges and Materials Processing* (New York: Wiley)

[19] Thompson J B 1959 Research Notes *Proc. R. Soc.* **73** 818
see also Rogoff G L 1985 *J. Phys. D: Appl. Phys.* **18** 1533
[20] Boyd R L F and Thompson J B 1959 *Proc. R. Soc.* A **252** 102
Braithwaite N St J and Allen J E 1988 *J. Phys. D: Appl. Phys.* **21** 1733
Riemann K U 1991 *J. Phys. D: Appl. Phys.* **24** 493
Boswell R W, Lichtenberg A J and Vender D 1992 *IEEE Trans. Plasma Sci.* **20** 62
[21] Godyak V A, Piejak R B and Alexandrovich B M 1992 *Plasma Sources Sci. Technol.* **1** 3
Godyak V A, Piejak R B and Alexandrovich B M 1999 *Plasma Sources Sci. Technol.* **8** 151
[22] Wang Z, Lichtenberg A J and Cohen R H 1998 *IEEE Trans. Plasma Sci.* **26** 59
Wang Z, Lichtenberg A J and Cohen R H 1999 *Plasma Sources Sci. Technol.* **8** 151